Accumulated Structural Evolution under Diurnal Cycling Degrades Wide-Bandgap Perovskite Solar Cells

Tonghan Zhao,[#] Mahmoud M. Elshanawany,[#] Roja Singh, Renjun Guo,[*] Bryce S. Richards,[*] and Ulrich W. Paetzold[*]

ABSTRACT: Mixed-halide wide-bandgap (WBG) perovskite thin films are prime candidate materials for next generation tandem perovskite photovoltaics. One major concern about this material class is the apparent halide phase segregation during operation, which reduces the operational lifetime. Here, we investigate the impact of phase segregation and crystallite orientation on the degradation of WBG perovskite films under a light/dark cycling mode. The photoluminescence of perovskite thin film presents a red-shift peak under illumination, then it exhibits a complete recovery to the initial position during storage in the dark, while *operando* structural evolution results reveal that light-induced lattice distortion, phase segregation, and phase reorientation only partially recover under the dark condition. These findings align with the observed partial recovery of the power conversion efficiency in the dark, demonstrating the accumulation of crystalline distortion and phase reorientation over light/dark operation is one of the significant causes for the performance loss in WBG perovskite solar cells.

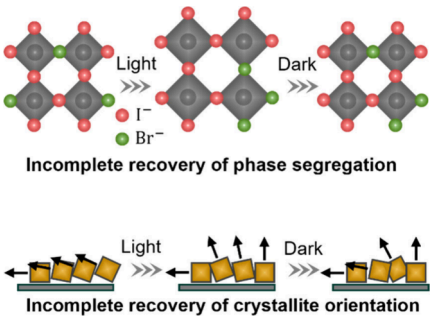

Over the past decade, metal halide perovskites have made extraordinary progress in solar cells,[1−4] light-emitting diodes (LED),[5−7] and photodetectors[2] due to their unique optoelectronic properties, high power conversion efficiency (PCE), low fabrication costs, and multiple fabrication methods.[8] Lead halide perovskites thin films serve as photovoltaic absorber layers in high performance devices, achieving record PCE of 26.95% for single-junction perovskite solar cells (PSCs).[9] Typical hybrid perovskites have a formula of $APbX_3$, consisting of formamidinium (FA^+), methylammonium (MA^+), or cesium (Cs^+) on the A site and halide ions (I^- or Br^-) on the X site.[10] State-of-the-art high-performance devices use triple-cation mixed-halide perovskites (e.g., $Cs_y(FA_zMA_{1-z})_{1-y}Pb(I_xBr_{1-x})_3$) as the light-absorbing layer.[11−13] Tuning the compositions of the A site has proven effective for improving the heat and moisture stability of perovskites.[14−16] One of the most influential improvements was the incorporation of Cs^+ to fine-tune the Goldschmidt tolerance factor toward a more structurally stable black phase perovskite.[17−19] For the X site, mixing I^- and Br^- anions allows direct bandgap energy (E_g) control between pure $APbI_3$ ($E_g \approx$ 1.5 eV) and $APbBr_3$ ($E_g \approx$ 2.4 eV), which has generated significant interest in developing wide-bandgap (WBG) perovskites.[20−22] These bandgap tunability and versatile processing routes make WBG perovskite thin films prime candidates for tandem photovoltaic devices,[23,24] leading to a record PCE of 34.6% and 30.1% for a perovskite/silicon tandem device and an all-perovskite tandem solar cell,[9] respectively. However, the stability of the WBG perovskites under light stress remains the main challenge due to the halide phase segregation.

Upon continuous illumination, mixed-halide perovskite thin films undergo halide ion migration-induced phase segregation, forming iodide-rich and bromide-rich phases. The iodide-rich domains trap adjacent carriers, leading to severe charge carrier recombination and bandgap shifts.[25−28] Consequently, light-induced halide phase segregation degrades device performance. Several models have been proposed to understand this phenomenon, including defect-driven halide ion movement,[29−31] polaron-induced local strain,[32] carrier-induced strain gradients,[33,34] local crystal misorientations,[35] hole trapping at iodide sites,[36,37] a two-state model in the excited state,[38] and overcoming entropy of halide intermixing with high-power excitation.[39,40] Interestingly, when the perovskite is

left in the dark, it gradually returns to its initial well-mixed state as thermal activation drives the segregated domains back to their original homogenized composition.[41] While multiple models provide explanations for the mechanisms driving phase segregation, the structural evolution such as lattice distortion, phase segregation, and phase reorientation that occur along with the phase degradation have not been studied systematically. Moreover, the correlation to the performance decline of the structural evolution effects is not yet comprehensive. Given that solar panels operate under natural day/night cycles, studying the role of light/dark cycling in halide phase segregation is essential.

In response, this study reports on triple-cation mixed-halide lead perovskite thin films that undergo significant lattice expansion and phase segregation, accompanied by changes in crystallite orientation, under intense exposure to light (~450 nm). In the absence of illumination, although its photoluminescence (PL) property returns to the initial state, both phase segregation and orientation are only partially recovered, as revealed by grazing-incidence wide-angle X-ray scattering (GIWAXS). With alternating light/dark exposure, phase segregation-coupled structure and texture variations gradually become irreversible and fixed. This corresponds with the observation that while the PCE partially recovers in the dark, the overall efficiency gradually decreases with the light/dark cycling. To summarize, by tracking the evolution of phase segregation and crystallite orientation in mixed-halide perovskites during light/dark cycling, this study demonstrates their gradual path toward irreversible degradation behaviors. These results provide critical evidence relevant to light-induced degradation of PSCs, highlighting the role of cumulative phase changes as a key factor influencing the long-term performance of PSCs.

To elucidate the impact of light soaking on the stability and underlying structural dynamics of the mixed-halide perovskite thin films, the evolution of crystalline phase is systematically investigated by combining PL and GIWAXS methods. PL measurements have the advantage of being highly sensitive to changes in the bandgap.[42,43] Typically, light-induced iodide-rich domains can cause characteristic redshifts in PL spectra, allowing us to readily observe the onset and temporal dynamics of phase segregation process. However, PL provides indirect information about the structural changes. GIWAXS measurements are employed to directly confirm the formation of segregated phases and crucially probe associated changes in lattice parameters and crystallite orientation,.[35,44] In the following section, this combined PL and GIWAXS approach allows for a comprehensive analysis of changes in energy band and crystalline structure that caused by phase segregation.

Time-dependent PL measurements at room temperature (298 K) provide insight into the photoexcitation-induced halide phase segregation dynamics in the triple-cation mixed-halide $Cs_{0.05}(FA_{0.77}MA_{0.23})_{0.95}Pb(I_{0.77}Br_{0.23})_3$ perovskite thin film. The perovskite film was fabricated on a (2-(9H-carbazol-9-yl)ethyl)phosphonic acid (2PACz)-coated indium tin oxide (ITO) glass substrate (Figure 1a) via the antisolvent method (see details in Supporting Information).[45] The WBG perovskite film shows high optical absorbance and exhibits a direct bandgap of E_g = 1.68 eV, which is calculated by using Tauc's relation (Figure S1). The surface morphological properties of the perovskite film are shown in Figure 1b. A scanning electron microscope (SEM) image reveals a uniformly distributed nanostructure forming a dense film. Figure 1c shows the PL

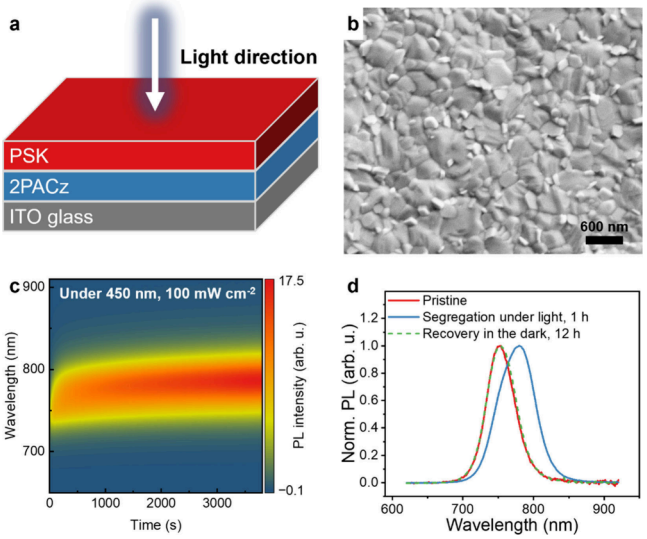

Figure 1. (a) Perovskite film on 2PACz-coated ITO glass. (b) Scanning electron microscopy (SEM) image of perovskite thin film. (c) Evolution of photoluminescence (PL) spectra of perovskite thin film upon illumination of 450 nm light with a power density of 100 mW cm^{-2}. (d) PL spectra of perovskite film at pristine, light-induced phase segregation and recovered statuses. The depicted phenomenon is representative and was consistently observed across three independent samples, with each experiment repeated three times.

spectra of the 1.68 eV perovskite film as a function of time upon illumination with 450 nm light (LED) at a power density of 100 mW cm^{-2}. It should be noted that while this power density numerically matches the intensity of the standard air-mass 1.5 global (AM 1.5G) solar spectrum, the near-monochromatic excitation at 450 nm results in a significantly higher photon flux density compared to the spectrally broad sunlight. This condition was chosen to effectively explore the halide segregation dynamics. The PL emission initially peaks at 753 nm before redshifting within 60 min and settling around 780 nm. A multiple-peak Gaussian fit of the PL spectra was used to further analyze this spectral evolution (Figure S2). The analysis reveals that the growing lower-energy emission is not a single feature but is composed of two distinct species: a red-shifted peak centered at 780 nm and a blue-shifted peak centered at 746 nm. The simultaneous emergence of these two peaks is a clear signature of light-induced phase segregation. The red-shifted peak corresponds to the formation of emissive iodide-rich domains. This observation is fully consistent with established models of phase segregation in mixed-halide perovskite films.[41,43] Moreover, the integrated PL intensity increased and remained at its maximum for a period, followed by a drop under long-term illumination (Figure S3a). The observed behavior is in good agreement with previous studies, which attribute the increase in PL intensity to the formation of highly emissive iodide-rich domains and the passivation of pre-existing nonradiative trap states.[30,41,43] This enhancement ceases once the phase segregation process reaches a steady state and other degradation pathways begin to dominate, leading to the subsequent quenching of the PL. The possibility of light-induced heating can be discounted. A control experiment demonstrates that upon heating the sample to 85 °C, the PL emission exhibits a blue-shift (Figure S4). This thermal behavior is contrary to the spectral changes observed

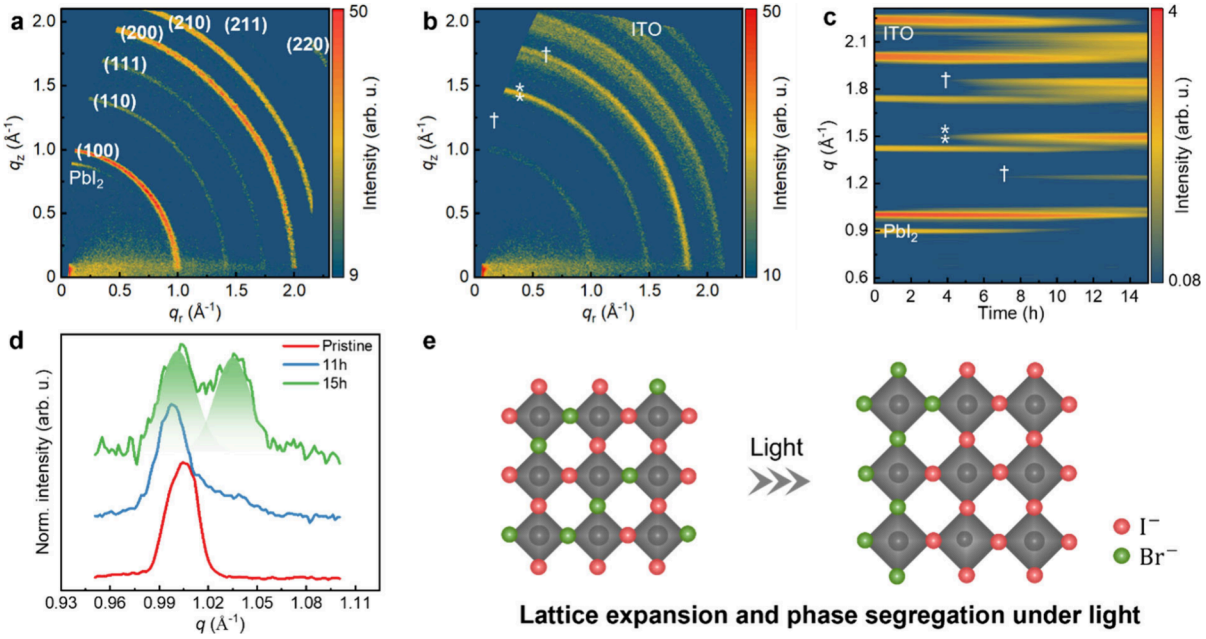

Figure 2. 2D GIWAXS images of (a) pristine perovskite film and (b) film upon irradiation of 450 nm light with a power density of 100 mW cm^{-2} for 15 h. (†) Hexagonal phase; (double asterisk) Mixed hexagonal phase and ITO. (c) X-ray scattering signal of perovskite film as a function of time upon illumination of 450 nm light with a power density of 100 mW cm^{-2}. (d) Pseudo XRD obtained from radical integral of 2D GIWAXS images of (100) plane in illumination times of 0, 11, and 15 h. (e) Schematic illustration of lattice expansion and phase segregation in perovskite film under light.

under illumination, indicating that heating is not the driving mechanism. SEM images reveal that the perovskite film exhibits numerous voids after light-soaking treatment (Figure S5). The formation of these features is attributed to the decomposition of the perovskite into volatile species.[46,47] The volatile byproducts of the perovskite thin film result in a net perovskite material loss, leading to the observed void creation. To investigate the influence of excitation power density on light-induced phase segregation, the PL was monitored under illumination at 1.6, 10, and 500 mW cm^{-2}. As shown in Figure S3, the rates of PL intensity saturation and emission peak shifting are strongly dependent on the excitation power. At lower power densities, these changes occur more slowly, whereas they are fastest at 500 mW cm^{-2}. These results demonstrate that segregation occurs across all tested power levels and the rate of phase segregation into iodide-rich and bromide-rich domains is directly correlated with the excitation power density. In addition, the local probing caused artifacts are ruled out by applied large-area (4 cm^2) PL measurement at 1.6 mW cm^{-2}. Both the rate at which the PL intensity saturates, and the kinetics of the spectral peak shift are in excellent agreement with the trends observed with a smaller spot size (Figure S6). Figure 1d reveals that phase segregation is reversible in darkness, with nearly complete recovery of the original PL emission spectra. However, the overall recovery process occurs on a much slower time scale than the light-induced phase segregation process. At room temperature, the segregated WBG perovskite film recovers completely in 12 h under dark conditions, indicating a low rate of spontaneous ion migration for halide remixing.[36] It should be noted that PL reveals phase segregation from a macroscopic property, yet further investigation is required to understand the manifestation of phase segregation within the perovskite structure.

To reveal the operando structural evolution of the perovskite film during exposure to light, *in situ* GIWAXS measurements were performed under light irradiation. The time evolution of two-dimensional (2D) GIWAXS data demonstrates remarkable phase segregation, generating iodide-rich and bromide-rich domains. The initial perovskite sample exhibited a characteristic cubic phase crystal structure (Figure 2a). After 15 h of illumination, its lattice structure underwent significant changes, transitioning into the hexagonal phase (Figure 2b). As depicted in Figure 2c,d, the scattering vector position of the (100) Bragg peak experiences a dramatic shift from 1.005 to 0.997 Å^{-1} after 11 h of illumination, indicating an increase in the interplane spacing of the crystal. This initial shift of the (100) Bragg peak position is followed by a slight back shift returning to 1.003 Å^{-1} and the emergence of a secondary peak at 1.036 Å^{-1}, coinciding with the phase segregation behavior.[10] Similar to the power-dependent effect on PL, low excitation power density can still cause phase segregation at a slower rate (Figure S7). To verify that phase segregation is caused by light, we stored the perovskite film in the dark for 74 days. The X-ray scattering results demonstrate that although part of the cubic phases transitioned to a thermodynamically stable hexagonal phase in air,[48,49] the initial peak position of the perovskite remained, and no splitting peak arose (Figure S8). This phenomenon confirms that halide phase segregation is triggered by light soaking.

It is well established that the phase segregation behavior in mixed-halide perovskites is influenced by multiple factors, including bromide content, surface morphology, and grain size.[50−54] Specifically, perovskite compositions with lower bromide fractions have been shown to exhibit slower segregation rates. The optical and structural properties of a perovskite with a relatively narrow bandgap $(Cs_{0.05}(FA_{0.90}MA_{0.10})_{0.95}Pb(I_{0.90}Br_{0.10})_3$, $E_G \approx 1.58$ eV) was thus studied under illumination. As shown in Figures S9 and S10, the bathochromic shift of PL and variation of the Bragg scattering peak are similar to the behaviors of the 1.68 eV

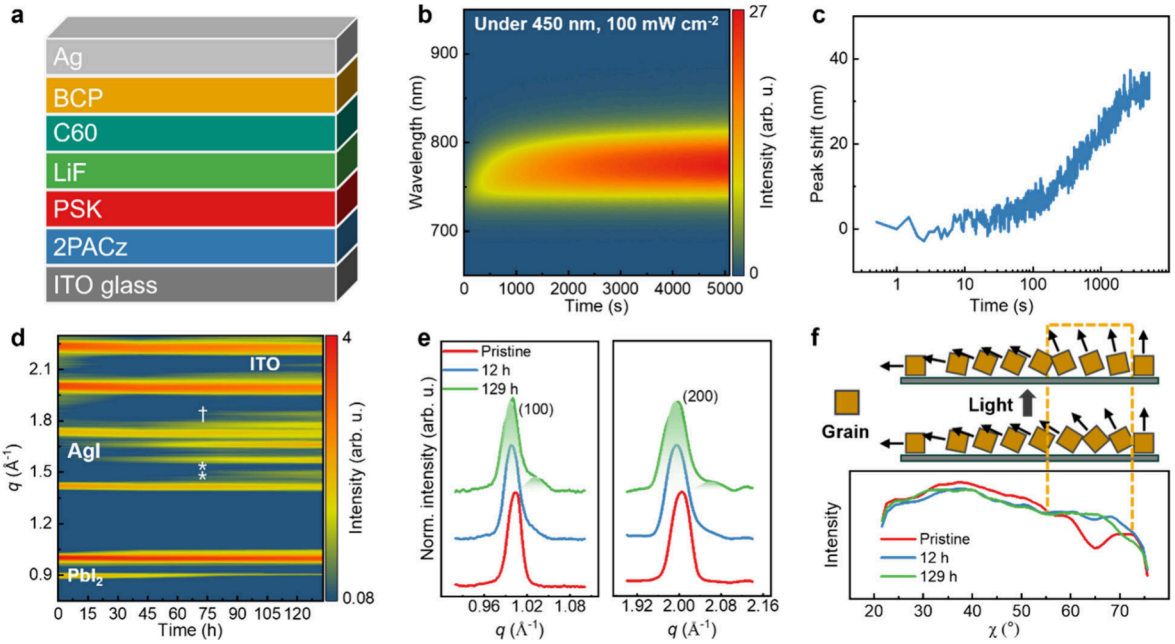

Figure 3. (a) Device architecture of PSCs. (b) Evolution of PL spectra of PSC device upon illumination of 450 nm light with a power density of 100 mW cm^{-2}. (c) Evolution of PL peaks upon illumination of 450 nm light with a power density of 100 mW cm^{-2}. (d) X-ray scattering signal of perovskite film as a function of time upon illumination of 450 nm light with a power density of 100 mW cm^{-2}. (†) Hexagonal phase; (double asterisk) Mixed hexagonal phase and ITO. (e) 1D scattering plots of (100) and (200) planes in illumination time of 0, 12, and 129 h. (f) Pole figures of (210) plane in illumination time of 0, 12, and 129 h. The schematic diagram shows the evolution of the orientation distribution of the crystallite grains.

perovskite, which can be attributed to the formation of separated iodide-rich and bromide-rich phases. Therefore, phase segregation can be caused by light in both types of perovskites. These results indicate that triple-cation mixed-halide perovskites experience lattice expansion and phase segregation upon irradiation (Figure 2e).

To gain a deeper understanding of how the overall stacking layers affect phase segregation in perovskite solar cells, we fabricated a single-junction device employing fullerene (C_{60})/bathocuproine (BCP) as the ETL and silver (Ag) as the electrode. Figure 3a presents the device architecture of the PSCs. Figure S11 shows the related performances for 19 devices, demonstrating a statistically average PCE of 20.69%. The time-tracking PL measurements show a significant peak shift from 742 to 780 nm (Figure 3b,c). The complete device exhibits enhanced photostability compared to the bare perovskite film, indicating a suppression of photoinduced phase segregation (Figure S12). The complete device exhibits enhanced photostability compared to the bare perovskite film, indicating a reduced photoinduced phase segregation (Figure S12). This improved stability can be attributed to the effect of the adjacent device layers, which act as a physical barrier, limiting the escape of volatile byproducts that are known to accelerate ion migration and phase segregation.[47]

The GIWAXS measurements assess the structural evolution in PSCs. It reveals that the phase segregation does not completely follow the pattern observed in the pure film. Typically, the cubic phase of perovskites remains after the deposition of the ETL and Ag electrode (Figure S13a). Upon illumination with 450 nm light, the Bragg peak of (100) shifts from 1.003 to 0.998 Å^{-1} in 12 h, then slightly shifts back to 1.000 Å^{-1} in 129 h, and the (200) peak shifts from 2.006 to 1.995 Å^{-1} in 12 h, then back to 1.998 Å^{-1} in 129 h (Figure 3d,e). This behavior is similar to that of the pure film. However, the shoulder peaks of (100) and (200) are much weaker compared to the pure film. This result indicates that the built-in electric field, which can separate both hole and electron, could significantly mitigate phase segregation. Additionally, the X-ray scattering spectrum from the PSC sample shows peaks at q = 1.571 and 1.668 Å^{-1} in 129 h (Figures 3d and S13b), which can be assigned to (100) and (002) of AgI, respectively. This phenomenon may be attributed to the ion migration of iodide, which then reacts with the Ag layer in the presence of oxygen and H_2O.[55,56] The reaction of the Ag electrode with I^- from the perovskite to form AgI is a degradation pathway in PSCs. Although a previous study reported the AgI can suppress the segregation,[57] silver is used as an external top electrode in our work, not as a dopant incorporated into the perovskite lattice. The interaction is therefore interfacial or diffusion of Ag rather than compositional.[58] This process is detrimental to the PCE and increases the hysteresis in current density–voltage (J–V) measurements (Figure S14). To mitigate this degradation, previous studies have proposed several strategies, including introducing an impermeable blocking layer between the perovskite and the electrode, or designing a metal alloy electrode to prevent the reaction of Ag^+ and I^-.[56,59] To differentiate between thermal and light-induced effects on PSCs degradation, we performed *in situ* GIWAXS measurement on a sample held at 85 °C in the dark. The measurement shows that the (100) Bragg peak shifts to a lower q value angle (q from 1.002 to 0.999 Å^{-1}), indicating lattice expansion, within the first 3 h, after which it remains stable for the entire 12 h experiment (Figure S15). Critically, no secondary peaks were observed during the heating process. This behavior is distinctly different from the phenomenon seen under illumination, where the emergence of new peaks signals phase segregation. Therefore, we conclude that while thermal stress contributes to lattice expansion, photoirradiation is the

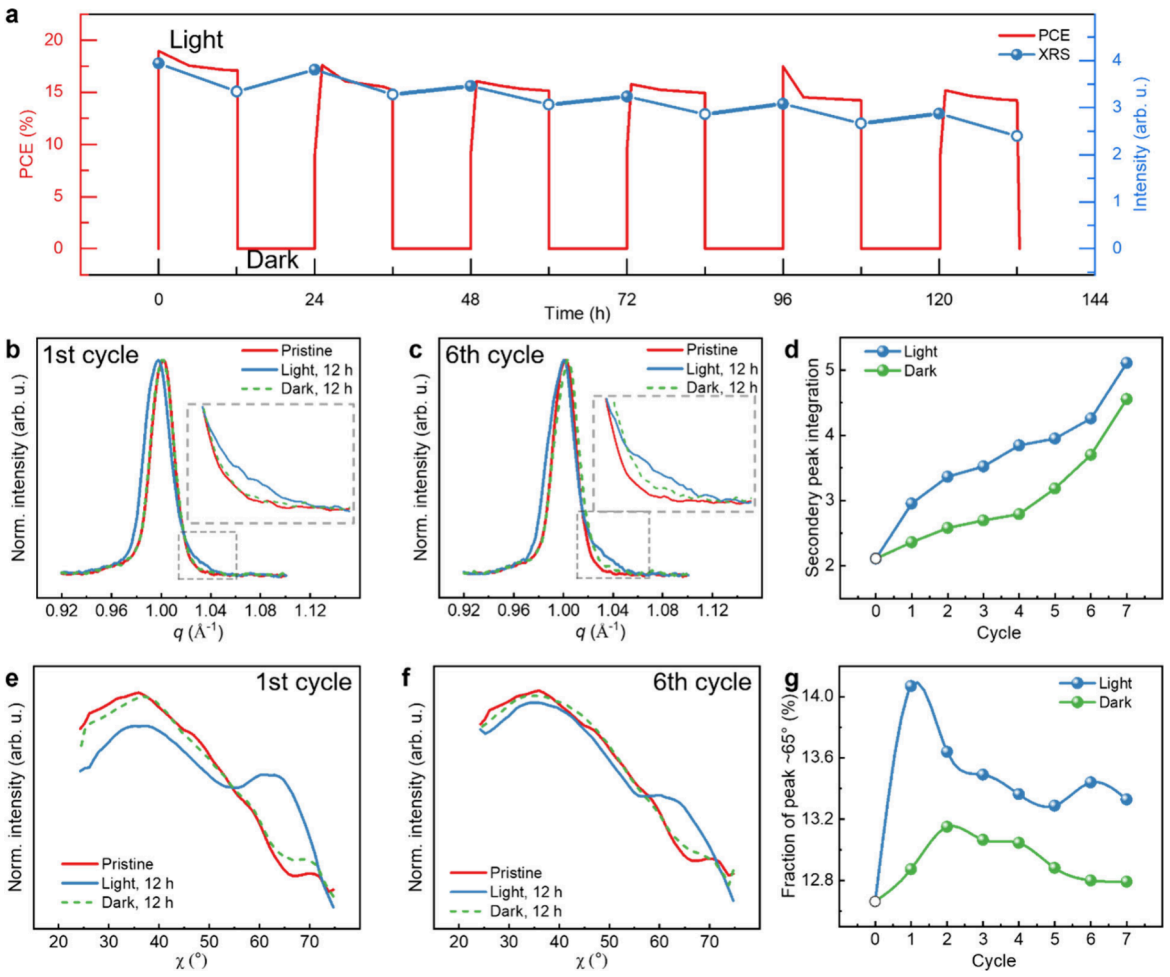

Figure 4. (a) Maximum power point tracking of the device and X-ray scattering intensity of (100) plane under six cycles of 12 h illumination/12 h dark. (b, c) 1D scattering plots of (100) plane in (b) the first light/dark cycle and (c) the sixth light/dark cycle. Inserts are the enlarged drawing from 1.016 to 1.072 Å^{-1}. (d) Evolution of the secondary peak under seven light/dark cycles. The intensities are integrated from 1.016 to 1.072 Å^{-1}. (e, f) Pole figures of (210) plane in (e) the first light/dark cycle and (f) the sixth light/dark cycle. (g) Fraction of the peak ~ 65° over the crystal orientation extracted from (210) plane under seven light/dark cycles.

primary driving force for phase segregation. We further used Williamson−Hall analysis to track the film strain evolution. As shown in Figure S16, the strain of the perovskite layer increases during illumination with 450 nm light. This rising structural strain may cause local crystal misorientation. Initially, the (100) plane was chosen for textural analysis. The pole figure derived from the (100) plane reveals a similar orientation distribution both before and during illumination (Figure S17). This observation is attributed to the crystallographic equivalence of the (100), (010), and (001) planes within a cubic phase, which makes it challenging to discern an orientation change between these planes in a pole figure. Therefore, the (210) plane was selected for subsequent analysis due to its comparatively high intensity among other Bragg peaks. As depicted in Figure 3f, the azimuthal angle of the (210) plane at approximately 65° increases under illumination. Based on the mutual crystallographic positions of the planes, this result suggests that the crystalline orientation distribution varys with a preferential alignment of the (010) plane parallel to the substrate surface during illumination. Based on these results, phase segregation is mitigated but cannot be completely prevented within a device stack. Additionally, light-induced strain in the perovskite thin film leading to the misorientation of perovskite phases is also expected to impact device performance.

Although constant illumination can induce phase segregation and texture reorganization in perovskite, solar panels operate under natural day/night cycling of temperature and light exposure in real world applications.[60,61] Khenkin et al. revealed that the stability of PSCs could be quite different under natural day/night cycling compared to constant illumination.[60] Therefore, it is crucial to understand the degradation differences between natural cycling and continuous modes. As shown in Figures 4 and S18, a 12 h light/dark cycling to simulate day/night operation of the devices was conducted. In this test, the cell was held at the maximum power point voltage (V_{mpp}) during the light part of the cycle. Consistent with previous reports, the PCE partially recovers during the dark period.[62,63] The PCE of the solar cell exhibits a total 25% decrease under continuous operation at V_{mpp} after six cycles of the 12-h light/dark test (Figure S19). Subsequently, we explored the evolution of structural spectra under light/dark cycling. Impressively, the scattering intensity of the (100) plane is also partially recoverable after dark storage (Figure 4a). Therefore, one of the reasons for the reversible behavior of PCE can be attributed to the self-healing process of the perovskite structure in the dark.[63,64]

To reveal whether the recovery of PCE in darkness relates to phase remixing, we investigate the evolution of Bragg peak position in light/dark cycle. As depicted in Figure 4b, the scattering vector q value of the (100) peak decreases from 1.002 to 0.998 $Å^{-1}$ after 12 h of illumination. Meanwhile, a small secondary peak appears at ~1.033 $Å^{-1}$, indicating phase segregation. Interestingly, after keeping the PSC in darkness for 12 h, the (100) peak returns to 1.002 $Å^{-1}$ and the secondary peak vanishes. Therefore, besides the PL behavior, lattice distortion and phase segregation are reversible in the first light/dark cycle. Nevertheless, with increasing treatment cycles, the peak position of (100) gradually shifts to a larger q value, either under illumination or in the dark (Figures 4c and S20). Additionally, the secondary peak becomes stronger (Figure 4d), indicating that phase segregation tends to become permanent over light/dark cycling. To investigate the cumulative impact of thermal stress, a thermal cycling experiment was conducted, alternating between 6 h of heating at 85 °C and 6 h at room temperature (RT). As shown in Figure S21, during the first cycle, the Bragg peak shifts to a smaller q-vector (q from 1.000 to 0.993 $Å^{-1}$), indicating lattice expansion. This expansion is irreversible, as the peak does not return to its original position upon cooling to RT. The lattice remains in this expanded state throughout six complete heating and cooling cycles. Crucially, no secondary peaks associated with phase segregation were detected at any point during the experiment. This result reinforces our previous conclusion: while thermal stress can cause an expansion of the perovskite lattice, light irradiation is the primary driving force for phase segregation.

As for phase orientation, Figure 4e shows that a peak at approximately 65° arises under continuous illumination. This peak weakens after 12 h of dark treatment, implying that the crystalline orientation of the perovskite film also undergoes an incomplete recovery process. During the cycling mode, the peak at ~65° increases first (either under illumination or in the dark), followed by gradual decrease and stabilization (Figure 4f,g). The orientation distribution of grains demonstrably changes with alternating light and dark exposure. After several cycles, the differences in grain orientation become slight, suggesting that cyclic exposure, rather than cumulative illumination, is the predominant factor governing orientation dynamics. Above all, both light-induced phase segregation and crystallite reorientation can return in the dark. As shown in Figure 5, the phase segregation and orientation change of PSC are partially reversible, leading to partial recovery of PCE performance in darkness. However, these effects accumulate over cycles, resulting in permanent PCE loss in the device.

The universality of light-induced phase segregation and partial recovery in darkness was further investigated using a white light source (WLED, 400–780 nm) on the 1.68 eV PSC. The total power density of the white light is ~100 mW cm^{-2}, which is comparable to that of 450 nm LED. It is important to note that the energy of the white light is distributed across a wide spectrum. This results in a considerably lower spectral power density at 450 nm and thus a lower effective photon flux capable of driving these structural changes compared to the high-intensity 450 nm irradiation. As shown in Figure S22a,b, the changes in lattice parameters and pole figure caused by the white light are not as significant as those induced by the 450 nm light, which is attributed to the distinct nature of the extinction. Despite the reduced magnitude, both lattice and orientation changes induced by white light still exhibited

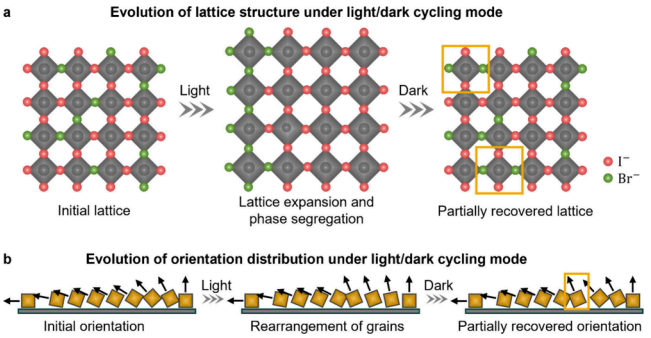

Figure 5. (a) Schematic diagram projecting the nonuniform lattice expansion and halide phase segregation of the WBG perovskites upon light illumination, followed by partial remixing of I^- and Br^- in darkness. (b) Schematic diagram of varying orientation distribution under light and its partial recovery in darkness. The differences of recovered structure and texture to initial state are highlighted by yellow frames.

partial recovery in darkness. Additionally, the light-soaking effect on 1.58 eV PSC was investigated. The 1.58 eV PSC under the same 450 nm light illumination shows a slight shift in the scattering vector, but its orientation exhibits preferential rearrangement upon illumination and then recovers in the dark (Figure S22c,d). Both the 1.58 and 1.68 eV PSCs exhibit reorientation toward approximately 65° under illumination. However, the extent of this orientation change is significantly less pronounced for the 1.58 eV PSC compared to the 1.68 eV PSC, probably attributed to their distinct compositions. Therefore, the observed partially reversible behaviors — encompassing phase segregation and orientation reorganization — appear to be general phenomena occurring under different light source types and in perovskites with different bandgaps, although the extent of these changes is clearly intensity- and spectrum-dependent.

In summary, this work reveals the light/dark cycling-dependent degradation mechanisms in WBG single-junction PSCs, identifying structural and orientational changes as crucial contributing factors. Under light, PSCs experience significant lattice expansion, spontaneous phase segregation, and phase reorientation of mixed-cation mixed-halide perovskites. Initially, these effects are reversible in the dark. However, after several light/dark cycles, these changes become stabilized, potentially causing device performance loss. Understanding these degradation mechanisms is crucial for developing strategies to enhance the operational stability of WBG perovskite films, thereby enabling their integration into high-efficiency tandem solar cells. Future research should focus on the fine-tuning of the perovskite lattice, for example, through compositional engineering with different cations. By carefully guiding the crystallization process, it may be possible to increase the activation energy barrier for detrimental processes like ion migration or lattice reorientation. Such an approach would improve the resilience of perovskite against the cumulative stress induced by cyclic day/night operation, leading to more robust and long-lasting devices.

Experimental details; Absorption spectra, SEM image, PL spectra, and GIWAXS of perovskite thin film and PSCs; $J-V$ curve and statistical performance of PSCs (PDF)

AUTHOR INFORMATION

Corresponding Authors

Renjun Guo − *Institute of Microstructure Technology, Karlsruhe Institute of Technology, 76344 Eggenstein-Leopoldshafen, Germany; Light Technology Institute, Karlsruhe Institute of Technology, 76131 Karlsruhe, Germany;* orcid.org/0000-0003-1116-3334; Email: renjun.guo@kit.edu

Bryce S. Richards − *Institute of Microstructure Technology, Karlsruhe Institute of Technology, 76344 Eggenstein-Leopoldshafen, Germany; Light Technology Institute, Karlsruhe Institute of Technology, 76131 Karlsruhe, Germany;* orcid.org/0000-0001-5469-048X; Email: bryce.richards@kit.edu

Ulrich W. Paetzold − *Institute of Microstructure Technology, Karlsruhe Institute of Technology, 76344 Eggenstein-Leopoldshafen, Germany; Light Technology Institute, Karlsruhe Institute of Technology, 76131 Karlsruhe, Germany;* orcid.org/0000-0002-1557-8361; Email: ulrich.paetzold@kit.edu

Authors

Tonghan Zhao − *Institute of Microstructure Technology, Karlsruhe Institute of Technology, 76344 Eggenstein-Leopoldshafen, Germany;* orcid.org/0000-0002-5300-1651

Mahmoud M. Elshanawany − *Institute of Microstructure Technology, Karlsruhe Institute of Technology, 76344 Eggenstein-Leopoldshafen, Germany; Light Technology Institute, Karlsruhe Institute of Technology, 76131 Karlsruhe, Germany;* orcid.org/0000-0001-9013-1263

Roja Singh − *Institute of Microstructure Technology, Karlsruhe Institute of Technology, 76344 Eggenstein-Leopoldshafen, Germany; Light Technology Institute, Karlsruhe Institute of Technology, 76131 Karlsruhe, Germany;* orcid.org/0000-0002-2202-3612

Author Contributions

# These authors contributed equally to this work (T.Z. and M.M.E.). The manuscript was written through contributions of all authors. All authors have given approval to the final version of the manuscript.

Notes

The authors declare no competing financial interest.

ACKNOWLEDGMENTS

Financial support by the Helmholtz Association via the Solar Technology Acceleration Platform (Solar TAP), the project Zeitenwende (Accelerated transfer of next-generation solar cells into mass production), and the program-oriented funding IV of the Helmholtz Association (Materials and Technologies for the Energy Transition, Topic 1: Photovoltaics and Wind Energy, Code: 38.01.04) is highly acknowledged. This study further receives financial support from the program "zukunft.-niedersachsen" by the Ministry of Science and Culture in Lower Saxony. Furthermore, the authors especially thank the whole "perovskite taskforce" at KIT for fruitful discussions and assistance.

REFERENCES

(1) Kojima, A.; Teshima, K.; Shirai, Y.; Miyasaka, T. Organometal Halide Perovskites as Visible-Light Sensitizers for Photovoltaic Cells. *J. Am. Chem. Soc.* **2009**, *131*, 6050.

(2) Liao, C. H.; Mahmud, M. A.; Ho-Baillie, A. W. Y. Recent progress in layered metal halide perovskites for solar cells, photodetectors, and field-effect transistors. *Nanoscale* **2023**, *15*, 4219−4235.

(3) Wang, T.; Zhang, Y.; Kong, W. Y.; Qiao, L.; Peng, B. G.; Shen, Z. C.; Han, Q. F.; Chen, H.; Yuan, Z. L.; Zheng, R. K.; Yang, X. D. Transporting holes stably under iodide invasion in efficient perovskite solar cells. *Science* **2022**, *377*, 1227−1231.

(4) Shao, Z. P.; Wang, Z. W.; Li, Z. P.; Fan, Y. P.; Meng, H. G.; Liu, R. R.; Wang, Y.; Hagfeldt, A.; Cui, G. L.; Pang, S. P. A Scalable Methylamine Gas Healing Strategy for High-Efficiency Inorganic Perovskite Solar Cells. *Angew. Chem., Int. Ed.* **2019**, *58*, 5587−5591.

(5) Tan, Z. K.; Moghaddam, R. S.; Lai, M. L.; Docampo, P.; Higler, R.; Deschler, F.; Price, M.; Sadhanala, A.; Pazos, L. M.; Credgington, D.; Hanusch, F.; Bein, T.; Snaith, H. J.; Friend, R. H. Bright light-emitting diodes based on organometal halide perovskite. *Nat. Nanotechnol.* **2014**, *9*, 687−692.

(6) Kim, Y. H.; Cho, H.; Heo, J. H.; Kim, T. S.; Myoung, N.; Lee, C. L.; Im, S. H.; Lee, T. W. Multicolored Organic/Inorganic Hybrid Perovskite Light-Emitting Diodes. *Adv. Mater.* **2015**, *27*, 1248−1254.

(7) Cho, H. C.; Jeong, S. H.; Park, M. H.; Kim, Y. H.; Wolf, C.; Lee, C. L.; Heo, J. H.; Sadhanala, A.; Myoung, N.; Yoo, S.; Im, S. H.; Friend, R. H.; Lee, T. W. Overcoming the electroluminescence efficiency limitations of perovskite light-emitting diodes. *Science* **2015**, *350*, 1222−1225.

(8) Stranks, S. D.; Snaith, H. J. Metal-halide perovskites for photovoltaic and light-emitting devices. *Nat. Nanotechnol.* **2015**, *10*, 391−402.

(9) NREL. Best Research-Cell Efficiency Chart. https://www.nrel.gov/pv/cell-efficiency.html (accessed 2025−07−27).

(10) Zhang, Z.; Chen, W.; Jiang, X.; Cao, J.; Yang, H.; Chen, H.; Yang, F.; Shen, Y.; Yang, H.; Cheng, Q.; Chen, X.; Tang, X.; Kang, S.; Ou, X.-m.; Brabec, C. J.; Li, Y.; Li, Y. Suppression of phase segregation in wide-bandgap perovskites with thiocyanate ions for perovskite/organic tandems with 25.06% efficiency. *Nat. Energy* **2024**, *9*, 592−601.

(11) Doherty, T. A. S.; Nagane, S.; Kubicki, D. J.; Jung, Y. K.; Johnstone, D. N.; Iqbal, A. N.; Guo, D. Y.; Frohna, K.; Danaie, M.; Tennyson, E. M.; Macpherson, S.; Abfalterer, A.; Anaya, M.; Chiang, Y. H.; Crout, P.; Ruggeri, F. S.; Collins, S.; Grey, C. P.; Walsh, A.; Midgley, P. A.; Stranks, S. D. Stabilized tilted-octahedra halide perovskites inhibit local formation of performance-limiting phases. *Science* **2021**, *374*, 1598.

(12) Saliba, M.; Matsui, T.; Seo, J. Y.; Domanski, K.; Correa-Baena, J. P.; Nazeeruddin, M. K.; Zakeeruddin, S. M.; Tress, W.; Abate, A.; Hagfeldt, A.; Grätzel, M. Cesium-containing triple cation perovskite solar cells: improved stability, reproducibility and high efficiency. *Energy Environ. Sci.* **2016**, *9*, 1989−1997.

(13) Shao, Z.; Meng, H.; Du, X.; Sun, X.; Lv, P.; Gao, C.; Rao, Y.; Chen, C.; Li, Z.; Wang, X.; Cui, G.; Pang, S. Cs4PbI6-Mediated Synthesis of Thermodynamically Stable FA0.15Cs0.85PbI3 Perovskite Solar Cells. *Adv. Mater.* **2020**, *32*, 2001054.

(14) Yuan, M. J.; Quan, L. N.; Comin, R.; Walters, G.; Sabatini, R.; Voznyy, O.; Hoogland, S.; Zhao, Y. B.; Beauregard, E. M.; Kanjanaboos, P.; Lu, Z. H.; Kim, D. H.; Sargent, E. H. Perovskite energy funnels for efficient light-emitting diodes. *Nat. Nanotechnol.* **2016**, *11*, 872−877.

(15) Anaya, M.; Galisteo-López, J. F.; Calvo, M. E.; Espinós, J. P.; Míguez, H. Origin of Light-Induced Photophysical Effects in Organic

Metal Halide Perovskites in the Presence of Oxygen. *J. Phys. Chem. Lett.* **2018**, *9*, 3891−3896.
(16) Andaji-Garmaroudi, Z.; Anaya, M.; Pearson, A. J.; Stranks, S. D. Photobrightening in Lead Halide Perovskites: Observations, Mechanisms, and Future Potential. *Adv. Energy Mater.* **2020**, *10*, 1903109.
(17) Abdi-Jalebi, M.; Andaji-Garmaroudi, Z.; Cacovich, S.; Stavrakas, C.; Philippe, B.; Richter, J. M.; Alsari, M.; Booker, E. P.; Hutter, E. M.; Pearson, A. J.; Lilliu, S.; Savenije, T. J.; Rensmo, H.; Divitini, G.; Ducati, C.; Friend, R. H.; Stranks, S. D. Maximizing and stabilizing luminescence from halide perovskites with potassium passivation. *Nature* **2018**, *555*, 497−501.
(18) Hu, Y. H.; Hutter, E. M.; Rieder, P.; Grill, I.; Hanisch, J.; Aygüler, M. F.; Hufnagel, A. G.; Handloser, M.; Bein, T.; Hartschuh, A.; Tvingstedt, K.; Dyakonov, V.; Baumann, A.; Savenije, T. J.; Petrus, M. L.; Docampo, P. Understanding the Role of Cesium and Rubidium Additives in Perovskite Solar Cells: Trap States, Charge Transport, and Recombination. *Adv. Energy Mater.* **2018**, *8*, 1703057.
(19) Elshanawany, M. M.; Ricciardulli, A. G.; Jeronimo-Rendon, J. J.; Saliba, M.; Wachtveitl, J.; Braun, M. Ultrafast Carrier Dynamics in Wide Band Gap Mixed-Cation Perovskites: Influence of the Cs Cation. *J. Phys. Chem. C* **2022**, *126*, 8787−8793.
(20) Macpherson, S.; Doherty, T. A. S.; Winchester, A. J.; Kosar, S.; Johnstone, D. N.; Chiang, Y. H.; Galkowski, K.; Anaya, M.; Frohna, K.; Iqbal, A. N.; Nagane, S.; Roose, B.; Andaji-Garmaroudi, Z.; Orr, K. W. P.; Parker, J. E.; Midgley, P. A.; Dani, K. M.; Stranks, S. D. Local nanoscale phase impurities are degradation sites in halide perovskites. *Nature* **2022**, *607*, 294−300.
(21) Wang, R.; Liu, X.; Yan, S.; Meng, N.; Zhao, X.; Chen, Y.; Li, H.; Qaid, S. M. H.; Yang, S.; Yuan, M.; He, T. Efficient wide-bandgap perovskite photovoltaics with homogeneous halogen-phase distribution. *Nat. Commun.* **2024**, *15*, 8899.
(22) Suchan, K.; Jacobsson, T. J.; Rehermann, C.; Unger, E. L.; Kirchartz, T.; Wolff, C. M. Rationalizing Performance Losses of Wide Bandgap Perovskite Solar Cells Evident in Data from the. *Adv. Energy Mater.* **2024**, *14*, 2303420.
(23) Aydin, E.; Allen, T. G.; De Bastiani, M.; Razzaq, A.; Xu, L. J.; Ugur, E.; Liu, J.; De Wolf, S. Pathways toward commercial perovskite/silicon tandem photovoltaics. *Science* **2024**, *383*, No. eadh3849.
(24) Allen, T. G.; Ugur, E.; Aydin, E.; Subbiah, A. S.; De Wolf, S. A Practical Efficiency Target for Perovskite/Silicon Tandem Solar Cells. *ACS Energy Lett.* **2025**, *10*, 238−245.
(25) Knight, A. J.; Wright, A. D.; Patel, J. B.; McMeekin, D. P.; Snaith, H. J.; Johnston, M. B.; Herz, L. M. Electronic Traps and Phase Segregation in Lead Mixed-Halide Perovskite. *ACS Energy Lett.* **2019**, *4*, 75−84.
(26) DuBose, J. T.; Kamat, P. V. TiO(2)-Assisted Halide Ion Segregation in Mixed Halide Perovskite Films. *J. Am. Chem. Soc.* **2020**, *142*, 5362−5370.
(27) Tiede, D. O.; Calvo, M. E.; Galisteo-Lopez, J. F.; Miguez, H. Local Rearrangement of the Iodide Defect Structure Determines the Phase Segregation Effect in Mixed-Halide Perovskites. *J. Phys. Chem. Lett.* **2020**, *11*, 4911−4916.
(28) Xiao, C. X.; Zhai, Y. X.; Song, Z. N.; Wang, K.; Wang, C. L.; Jiang, C. S.; Beard, M. C.; Yan, Y. F.; Al-Jassim, M. Operando Characterizations of Light-Induced Junction Evolution in Perovskite Solar Cells. *ACS Appl. Mater. Interfaces* **2023**, *15*, 20909−20916.
(29) Azpiroz, J. M.; Mosconi, E.; Bisquert, J.; De Angelis, F. Defect migration in methylammonium lead iodide and its role in perovskite solar cell operation. *Energy Environ. Sci.* **2015**, *8*, 2118−2127.
(30) Barker, A. J.; Sadhanala, A.; Deschler, F.; Gandini, M.; Senanayak, S. P.; Pearce, P. M.; Mosconi, E.; Pearson, A. J.; Wu, Y.; Kandada, A. R. S.; Leijtens, T.; De Angelis, F.; Dutton, S. E.; Petrozza, A.; Friend, R. H. Defect-Assisted Photoinduced Halide Segregation in Mixed-Halide Perovskite Thin Films. *ACS Energy Lett.* **2017**, *2*, 1416−1424.
(31) Singh, R.; Hu, H.; Feeney, T.; Diercks, A.; Laufer, F.; Li, Y.; Duong, T.; Schackmar, F.; Nejand, B. A.; Paetzold, U. W. Danger in the Dark: Stability of Perovskite Solar Cells with Varied Stoichiometries and Morphologies Stressed at Various Conditions. *ACS Appl. Mater. Interfaces* **2024**, *16*, 27450−27462.
(32) Bischak, C. G.; Wong, A. B.; Lin, E.; Limmer, D. T.; Yang, P. D.; Ginsberg, N. S. Tunable Polaron Distortions Control the Extent of Halide Demixing in Lead Halide Perovskites. *J. Phys. Chem. Lett.* **2018**, *9*, 3998−4005.
(33) Slotcavage, D. J.; Karunadasa, H. I.; McGehee, M. D. Light-Induced Phase Segregation in Halide-Perovskite Absorbers. *ACS Energy Lett.* **2016**, *1*, 1199−1205.
(34) Ruth, A.; Brennan, M. C.; Draguta, S.; Morozov, Y.; Zhukovskyi, M.; Janko, B.; Zapol, P.; Kuno, M. Vacancy-Mediated Anion Photosegregation Kinetics in Mixed Halide Hybrid Perovskites: Coupled Kinetic Monte Carlo and Optical Measurements. *ACS Energy Lett.* **2018**, *3*, 2321−2328.
(35) Guo, R.; Han, D.; Chen, W.; Dai, L.; Ji, K.; Xiong, Q.; Li, S.; Reb, L. K.; Scheel, M. A.; Pratap, S.; Li, N.; Yin, S.; Xiao, T.; Liang, S.; Oechsle, A. L.; Weindl, C. L.; Schwartzkopf, M.; Ebert, H.; Gao, P.; Wang, K.; Yuan, M.; Greenham, N. C.; Stranks, S. D.; Roth, S. V.; Friend, R. H.; Müller-Buschbaum, P. Degradation mechanisms of perovskite solar cells under vacuum and one atmosphere of nitrogen. *Nat. Energy* **2021**, *6*, 977−986.
(36) Yoon, S. J.; Draguta, S.; Manser, J. S.; Sharia, O.; Schneider, W. F.; Kuno, M.; Kamat, P. V. Tracking Iodide and Bromide Ion Segregation in Mixed Halide Lead Perovskites during Photoirradiation. *ACS Energy Lett.* **2016**, *1*, 290−296.
(37) Draguta, S.; Sharia, O.; Yoon, S. J.; Brennan, M. C.; Morozov, Y. V.; Manser, J. M.; Kamat, P. V.; Schneider, W. F.; Kuno, M. Rationalizing the light-induced phase separation of mixed halide organic-inorganic perovskites. *Nat. Commun.* **2017**, *8*, 200.
(38) Belisle, R. A.; Bush, K. A.; Bertoluzzi, L.; Gold-Parker, A.; Toney, M. F.; McGehee, M. D. Impact of Surfaces on Photoinduced Halide Segregation in Mixed-Halide Perovskites. *ACS Energy Lett.* **2018**, *3*, 2694−2700.
(39) Elmelund, T.; Seger, B.; Kuno, M.; Kamat, P. V. How Interplay between Photo and Thermal Activation Dictates Halide Ion Segregation in Mixed Halide Perovskites. *ACS Energy Lett.* **2020**, *5*, 56−63.
(40) Yoon, S. J.; Kuno, M.; Kamat, P. V. How Halide Ion Defects Influence Photoinduced Segregation in Mixed Halide Perovskites. *ACS Energy Lett.* **2017**, *2*, 1507−1514.
(41) Gautam, S. K.; Kim, M.; Miquita, D. R.; Bourée, J. E.; Geffroy, B.; Plantevin, O. Reversible Photoinduced Phase Segregation and Origin of Long Carrier Lifetime in Mixed-Halide Perovskite Films. *Adv. Funct. Mater.* **2020**, *30*, 2002622.
(42) Brennan, M. C.; Draguta, S.; Kamat, P. V.; Kuno, M. Light-Induced Anion Phase Segregation in Mixed Halide Perovskites. *ACS Energy Lett.* **2018**, *3*, 204−213.
(43) Hoke, E. T.; Slotcavage, D. J.; Dohner, E. R.; Bowring, A. R.; Karunadasa, H. I.; McGehee, M. D. Reversible photo-induced trap formation in mixed-halide hybrid perovskites for photovoltaics. *Chem. Sci.* **2015**, *6*, 613−617.
(44) Qin, M. C.; Chan, P. F.; Lu, X. H. A Systematic Review of Metal Halide Perovskite Crystallization and Film Formation Mechanism Unveiled by In Situ GIWAXS. *Adv. Mater.* **2021**, *33*, 2105290.
(45) Al-Ashouri, A.; Köhnen, E.; Li, B.; Magomedov, A.; Hempel, H.; Caprioglio, P.; Márquez, J. A.; Vilches, A. B. M.; Kasparavicius, E.; Smith, J. A.; Phung, N.; Menzel, D.; Grischek, M.; Kegelmann, L.; Skroblin, D.; Gollwitzer, C.; Malinauskas, T.; Jost, M.; Matic, G.; Rech, B.; Schlatmann, R.; Topic, M.; Korte, L.; Abate, A.; Stannowski, B.; Neher, D.; Stolterfoht, M.; Unold, T.; Getautis, V.; Albrecht, S. Monolithic perovskite/silicon tandem solar cell with > 29% efficiency by enhanced hole extraction. *Science* **2020**, *370*, 1300.
(46) Zhang, D.; Li, D.; Hu, Y.; Mei, A.; Han, H. Degradation pathways in perovskite solar cells and how to meet international standards. *Commun. Mater.* **2022**, *3*, 58.
(47) Zhu, H. W.; Teale, S.; Lintangpradipto, M. N.; Mahesh, S.; Chen, B.; McGehee, M. D.; Sargent, E. H.; Bakr, O. M. Long-term

operating stability in perovskite photovoltaics. *Nat. Rev. Mater.* **2023**, *8*, 569−586.
(48) Jiang, S. J.; Luan, Y. L.; Jang, J. I.; Baikie, T.; Huang, X.; Li, R. P.; Saouma, F. O.; Wang, Z. W.; White, T. J.; Fang, J. Y. Phase Transitions of Formamidinium Lead Iodide Perovskite under Pressure. *J. Am. Chem. Soc.* **2018**, *140*, 13952−13957.
(49) Han, Q. F.; Bae, S. H.; Sun, P. Y.; Hsieh, Y. T.; Yang, Y.; Rim, Y. S.; Zhao, H. X.; Chen, Q.; Shi, W. Z.; Li, G.; Yang, Y. Single Crystal Formamidinium Lead Iodide (FAPbI): Insight into the Structural, Optical, and Electrical Properties. *Adv. Mater.* **2016**, *28*, 2253−2258.
(50) Wright, A. D.; Patel, J. B.; Johnston, M. B.; Herz, L. M. Temperature-Dependent Reversal of Phase Segregation in Mixed-Halide Perovskites. *Adv. Mater.* **2023**, *35*, No. e2210834.
(51) Suchan, K.; Just, J.; Beblo, P.; Rehermann, C.; Merdasa, A.; Mainz, R.; Scheblykin, I. G.; Unger, E. Multi-Stage Phase-Segregation of Mixed Halide Perovskites under Illumination: A Quantitative Comparison of Experimental Observations and Thermodynamic Models. *Adv. Funct. Mater.* **2023**, *33*, 2206047.
(52) Gualdrón-Reyes, A. F.; Yoon, S. J.; Barea, E. M.; Agouram, S.; Muñoz-Sanjosé, V.; Meléndez, A. M.; Niño-Gómez, M. E.; Mora-Seró, I. Controlling the Phase Segregation in Mixed Halide Perovskites through Nanocrystal Size. *ACS Energy Lett.* **2019**, *4*, 54−62.
(53) Hu, L.; Guan, X. W.; Chen, W. J.; Yao, Y. C.; Wan, T.; Lin, C. H.; Pham, N. D.; Yuan, L.; Geng, X.; Wang, F.; Huang, C. Y.; Yuan, J. Y.; Cheong, S. S.; Tilley, R. D.; Wen, X. M.; Chu, D. W.; Huang, S. J.; Wu, T. Linking Phase Segregation and Photovoltaic Performance of Mixed-Halide Perovskite Films through Grain Size Engineering. *ACS Energy Lett.* **2021**, *6*, 1649−1658.
(54) Tang, J. B.; Tian, W. M.; Sun, F. K.; Sun, Q.; Leng, J.; Zhao, S. L.; Jin, S. Y. Morphology-Dependent Carrier Accumulation Dynamics in Mixed Halide Perovskite Thin Films Caused by Phase Segregation. *J. Phys. Chem. Lett.* **2023**, *14*, 2800−2806.
(55) Li, J. W.; Dong, Q. S.; Li, N.; Wang, L. D. Direct Evidence of Ion Diffusion for the Silver-Electrode-Induced Thermal Degradation of Inverted Perovskite Solar Cells. *Adv. Energy Mater.* **2017**, *7*, 1602922.
(56) Kato, Y.; Ono, L. K.; Lee, M. V.; Wang, S. H.; Raga, S. R.; Qi, Y. B. Silver Iodide Formation in Methyl Ammonium Lead Iodide Perovskite Solar Cells with Silver Top Electrodes. *Adv. Mater. Interfaces* **2015**, *2*, 1500195.
(57) Hu, L.; Guan, X. W.; Wan, T.; Lin, C. H.; Liu, S. Q.; Zhu, R. B.; Chen, W. J.; Yao, Y.; Huang, C. Y.; Yuan, L.; Shahrokhi, S.; Chu, D. W.; Cazorla, C.; Chen, J. F.; Yang, J.; Yi, J. B.; Huang, S. J.; Wu, T. Valence-Regulated Metal Doping of Mixed-Halide Perovskites to Modulate Phase Segregation and Solar Cell Performance. *ACS Energy Lett.* **2022**, *7*, 4150−4160.
(58) Bastos, J. P.; Manghooli, S.; Jaysankar, M.; Tait, J. G.; Qiu, W. M.; Gehlhaar, R.; De Volder, M.; Uytterhoeven, G.; Poortmans, J.; Paetzold, U. W. Low-cost electrodes for stable perovskite solar cells. *Appl. Phys. Lett.* **2017**, *110*, na.
(59) Svanström, S.; Jacobsson, T. J.; Boschloo, G.; Johansson, E. M. J.; Rensmo, H.; Cappel, U. B. Degradation Mechanism of Silver Metal Deposited on Lead Halide Perovskites. *ACS Appl. Mater. Interfaces* **2020**, *12*, 7212−7221.
(60) Khenkin, M.; Köbler, H.; Remec, M.; Roy, R.; Erdil, U.; Li, J. Z.; Phung, N.; Adwan, G.; Paramasivam, G.; Emery, Q.; Unger, E.; Schlatmann, R.; Ulbrich, C.; Abate, A. Light cycling as a key to understanding the outdoor behaviour of perovskite solar cells. *Energy Environ. Sci.* **2024**, *17*, 602−610.
(61) Shen, Y.; Zhang, T.; Xu, G.; Steele, J. A.; Chen, X.; Chen, W.; Zheng, G.; Li, J.; Guo, B.; Yang, H.; Wu, Y.; Lin, X.; Alshahrani, T.; Yin, W.; Zhu, J.; Wang, F.; Amassian, A.; Gao, X.; Zhang, X.; Gao, F.; Li, Y.; Li, Y. Strain regulation retards natural operation decay of perovskite solar cells. *Nature* **2024**, *635*, 882−889.
(62) Peng, J.; Wu, Y.; Ye, W.; Jacobs, D. A.; Shen, H.; Fu, X.; Wan, Y.; Duong, T.; Wu, N.; Barugkin, C.; Nguyen, H. T.; Zhong, D.; Li, J.; Lu, T.; Liu, Y.; Lockrey, M. N.; Weber, K. J.; Catchpole, K. R.; White, T. P. Interface passivation using ultrathin polymer-fullerene films for high-efficiency perovskite solar cells with negligible hysteresis. *Energy Environ. Sci.* **2017**, *10*, 1792−1800.
(63) Domanski, K.; Roose, B.; Matsui, T.; Saliba, M.; Turren-Cruz, S. H.; Correa-Baena, J. P.; Roldán-Carmona, C.; Richardson, G.; Foster, J. M.; De Angelis, F.; Ball, J. M.; Petrozza, A.; Mine, N.; Nazeeruddin, M. K.; Tress, W.; Grätzel, M.; Steiner, U.; Hagfeldt, A.; Abate, A. Migration of cations induces reversible performance losses over day/night cycling in perovskite solar cells. *Energy Environ. Sci.* **2017**, *10*, 604−613.
(64) Nie, W.; Blancon, J. C.; Neukirch, A. J.; Appavoo, K.; Tsai, H.; Chhowalla, M.; Alam, M. A.; Sfeir, M. Y.; Katan, C.; Even, J.; Tretiak, S.; Crochet, J. J.; Gupta, G.; Mohite, A. D. Light-activated photocurrent degradation and self-healing in perovskite solar cells. *Nat. Commun.* **2016**, *7*, 11574.